Rechargeable Aqueous Zn2+-Battery with High Power Density and Long Cycle-life

Journal:	*Energy & Environmental Science*
Manuscript ID	EE-COM-06-2018-001883.R2
Article Type:	Communication
Date Submitted by the Author:	02-Oct-2018

Complete List of Authors:	Wang, Fei; U.S.Army Research Lab; University of Maryland Hu, Enyuan; Brookhaven national lab., ; Brookhaven National Laboratory, Chemistry Department Sun, Wei; University of Maryland Center for Environmental Science, Gao, Tao; University of Maryland, Chemical Engineering Ji, Xiao; University of Maryland, Department of Chemical & Biomolecular Engineering; Huazhong University of Science and Technology Tongji Medical College, Fan, Xiulin; University of Maryland, Department of Chemical & Biomolecular Engineering Han, Fudong; University of Maryland at College Park, Department of Chemical and Biomolecular Engineering Yang, Xiao-Qing; Brookhaven National Lab, Chemistry Xu, Kang; U. S. Army Research Laboratory, Electrochemistry Branch Wang, Chunsheng; University of Maryland, Department of Chemical & Biomolecular Engineering

Multi-valent (MV) battery chemistries have aroused intense interests recently. Among them, Zn-ion batteries are promising due to the practically abundant, high volumetric energy density and intrinsic safety. However, the Zn-ion host suffers from the sluggish diffusion due to its strong electrostatic interaction with host lattices. As consequence, Zn-ion insertion cathodes reported up to date are characterized of low working potential or poor reversibility. Those compromises constitute constant hurdle to essentially all MV batteries, limiting their practical applications. On the other hand, higher operating potentials of cathode usually come with lattice of stronger ionic nature, which inevitably present higher energy barriers for MV cation diffusions, further worsening the situation. In this work, we demonstrated that the polyanion structure with one-dimensional channel could enable the ultrafast and reversible Zn^{2+}-intercalation/de-intercalation at a high working voltage. The facile diffusion was achieved by delocalizing the nominal bivalence of the inserted Zn-ion over multiple atoms through the *p*-*d* hybridization between the V-*d* and O-*p* orbitals. The inserted Zn^{2+} has an effective charge of 1.336, rendering its high mobility. A direct correlation between the electronic structure and the Zn^{2+}-mobility in the bulk structure was also established, which could provide solutions for other MV batteries.

Journal Name

COMMUNICATION

Rechargeable Aqueous Zn2+-Battery with High Power Density and Long Cycle-life

Received 00th January 20xx,
Accepted 00th January 20xx

DOI: 10.1039/x0xx00000x

www.rsc.org/

Fei Wang,‡[a,b] Enyuan Hu, ‡[c] Wei Sun, ‡[a] Tao Gao, [a] Xiao Ji,[a] Xiulin Fan, [a] Fudong Han, [a] Xiao-Qing Yang,*[c] Kang Xu* [b] and Chunsheng Wang*[a]

Li-ion batteries (LIBs) are approaching their energy limits imposed by the intercalation chemistry nature. As alternatives, multivalent (MV) chemistries bring both promises and challenges, with the main obstacle being the sluggish diffusion of MV-cations due to their strong electrostatic interaction with host lattices. In this work, we demonstrated that polyanion based robust crystal architecture could enable the ultrafast and reversible Zn^{2+}-intercalation and de-intercalation at a high working voltage. The nominal bivalence of Zn^{2+} was successfully delocalized by the multiple atoms through the *p-d* hybridization between the V-*d* and O-*p* orbitals, hence the inserted Zn^{2+} only bears an effective charge of 1.336, rendering its high mobility. The novel aqueous rechargeable 1.7 V $Zn/LiV_2(PO_4)_3$ cell based on such mechanism delivers a high power density (8000 W/kg at 60 C) comparable to supercapacitors, a high energy density (218 Wh/Kg at 1 C) close to LIBs, with extraordinary long cycle life of 4000 cycles. All of these parameters far exceed any Zn battery reported so far. The cell-level volumetric and specific energy densities of the $Zn/LiV_2(PO_4)_3$ cell are 320 Wh/L and 150 Wh/kg, respectively, which are even better than the first-generation LIBs. Combining with the intrinsic safety of the aqueous chemistry and the wide working temperature range, this cell makes a strong candidate for automotive applications.

Rechargeable batteries are playing increasingly important roles in our mobile digital life, and their future applications in electric vehicles and grid-storage systems not only require higher energy density but more importantly better safety and lower cost. [1-4]. While Li-ion batteries (LIBs) are approaching their energy limits imposed by the intercalation chemistry nature and raising both safety and availability concerns, multivalent (MV) chemistries bring both promises and challenges, blessed by the transfer of multiple number of electrons during reduction/oxidation of each MV ion, but plagued by the sluggish diffusion of MV cations due to their strong electrostatic interaction with the host lattices. Despite potential high capacity, all MV insertion cathodes reported up to date typically suffer from low voltage, poor reversibility and especially sluggish kinetics[5-7].

Zinc (Zn) has one of the highest volumetric capacities (5851 mAh cm^{-3} vs. 2046 mAh cm^{-3} for Li metal, Figure S1), very high abundance in earth-crust globally, and good compatibility with aqueous electrolytes [5, 8] that confers intrinsic safety on Zn batteries [9-13]. In fact, it has been widely used as anode materials for primary systems ever since the dawn of batteries. Due to the same constraints that all other MV chemistries subject to, aqueous Zn batteries typically deliver much lower energy/power densities and poorer cycle life when compared to LIBs [10, 11, 14-21]. To date, facile Zn^{2+}-intercalation chemistry can only be enabled in simple transition metal oxides with open structure and two dimensional channels, which usually operate at low voltages. It was hence believed that the desirable high voltage of Zn^{2+}-intercalation would only be possible with those transition-metal oxides of highly ionic structure, which unfortunately comes with intrinsically high energy barriers for Zn^{2+}-diffusion [5,8,11,18]

To enable high rate capability for Zn chemistry, the desired cathode host should have a robust crystal architecture allowing fast and reversible Zn^{2+} (de-)intercalation. Such frameworks could be available from transition metal polyanion-based materials, which offers minimum steric hindrance, and whose intercalation potentials can be manipulated through the 3d-metal $M^{n+/}M^{n+1}$ redox couple (Figure S2) [22]. So far, however, reasonable cation diffusion and structural stability was only observed for certain transition metal polyanion-based materials that accommodates monovalent ion Li^+ [23, 24]. For example, in 1M Li_2SO_4-$ZnSO_4$ aqueous electrolytes, $Li_3V_2(PO_4)_3$ was shown to allow Li^+- instead of Zn^{2+}-intercalation to proceed reversibly, leading to a hybrid battery chemistry of $Zn/Li_3V_2(PO_4)_3$ [25].

Herein, overturning the traditional belief, we report for the first time that reversible Zn^{2+}-intercalation chemistry can be realized in a close-stacked lattice structure of one-dimensional channel with

[a] *Department of Chemical and Biomolecular Engineering, University of Maryland, College Park , MD 20742 , USA*
[b] *Electrochemistry Branch, Sensor and Electron Devices Directorate, Power and Energy Division, U.S. Army Research Laboratory, Adelphi, MD 20783, USA.*
[c] *Chemistry Division, Brookhaven National Laboratory, Upton, NY 11973, USA*
† Fei Wang, Enyuan Hu and Wei Sun contributed equally to this work.
Electronic Supplementary Information (ESI) available: [details of any supplementary information available should be included here]. See DOI: 10.1039/x0xx00000x

extreme fast rate and exceptional reversibility. Using $LiV_2(PO_4)_3$ as a starting template for cathode host, we demonstrated a 1.7 V new aqueous rechargeable $Zn/LiV_2(PO_4)_3$ cell that delivers a high power density (8000 W/kg) comparable to supercapacitors, a high energy density (218 Wh/Kg) close to LIBs, with extraordinary long cycle life of 4000 cycles. All these parameters far exceed those of any Zn battery known thus far. Detailed structural characterization and first principle calculation revealed that the facile diffusion was achieved by delocalizing the nominal bivalence of the inserted Zn-ion over multiple atoms through the p-d hybridization between the V-d and O-p orbitals, thus a large and open channel is no longer necessary. The significant performance improvements obtained in this work for the new $Zn/LiV_2(PO_4)_3$ chemistry and the in-depth understanding will provide valuable guidance to the research and development of rechargeable MV battery chemistries that have remained formidable challenges to researchers in materials and electrochemistry.

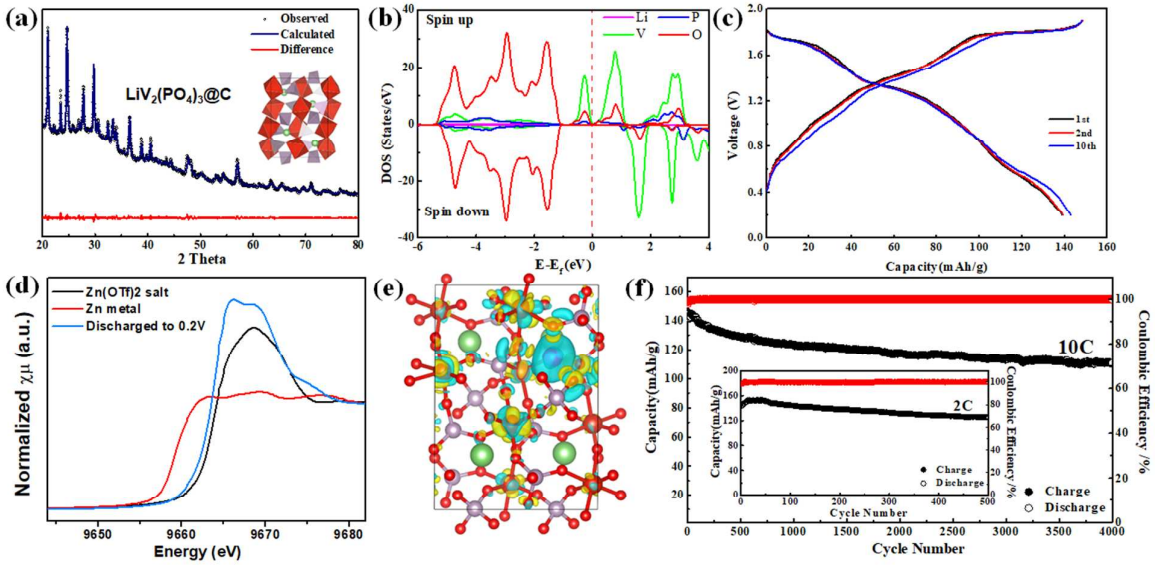

Figure 1. Structure of $LiV_2(PO_4)_3$ and its electrochemical behavior. (a) The XRD pattern and its Rietveld refinement results of the $LiV_2(PO_4)_3$@C prepared through the electrochemical delithiation process. (b) The partial density of states (DOS) for $LiV_2(PO_4)_3$. (c) The typical voltage profile of $Zn/LiV_2(PO_4)_3$ cell between 0.2 V and 1.9 V in the 4 m $Zn(OTf)_2$ electrolyte at ambient temperature at 2 C rate (1 C: 150mA/g, electrode areal mass loading: 10 mg/cm^2). (d) The XANES spectra collected at the Zn K-edge of the Zn metal, $Zn(OTf)_2$ salt and the LiV2(PO4)3 electrode discharged to 0.2 V. (e) The schematic illustration of change in charge distribution after Zn^{2+}-insertion into the $LiV_2(PO_4)_3$ framework (Blue: charge decrease; Yellow: charge increase). (f) The cycling performance and the corresponding coulombic efficiency at a high rate of 10 C (inset the low rate of 2 C).

The $Li_3V_2(PO_4)_3$@C composite was synthesized through a spray-drying method[26]. All XRD peaks are well indexed with monoclinic structure of $Li_3V_2(PO_4)_3$ where three lithium atoms occupy three distinct crystallographic positions (Figure S3)[27-31]. Electron microscopy characterizations demonstrate that the 100 nm $Li_3V_2(PO_4)_3$ primary particles are covered by the pyrolytic carbon and aggregated into 3 μm spherical secondary particles within a pyrolytic carbon matrix (Figure S4 & S5). The Zn^{2+}-intercalation host $LiV_2(PO_4)_3$ was synthesized by in-situ electrochemical extraction of two Li^+ ions from each $Li_3V_2(PO_4)_3$ formula unit under galvanostatic condition with careful controlling of charge voltage (Figure S6) [29, 32]. The formation of $LiV_2(PO_4)_3$ host was confirmed by XRD patterns where only one lithium site was retained in the formula, leaving two unoccupied site for the incoming Zn^{2+} (Figure 1a). 4 mol/kg (m, molality) zinc trifluoromethanesulfonate ($Zn(OTf)_2$) solution was used as electrolyte, which has a anodic stability limit of ~2.0 V vs Zn (~1.2 V vs standard hydrogen electrode (SHE), Figure S7). It has been reported that the electronic structure, reflected by the density of states (DOS)[7], is critical for the MV chemistry. Therefore, it was calculated for $LiV_2(PO_4)_3$ using first principle calculation. As shown in Figure 1b, The V-d and O-p orbital show obvious *p-d* hybridization, meaning the electrons introduced by the Zn^{2+}-intercalation in $LiV_2(PO_4)_3$ are well accommodated by both V and O sites. The very narrow band gap (~0.1 eV) of $LiV_2(PO_4)_3$ renders a high electronic conductivity when external electrical field is applied [33, 34]. The quick electron motion is critical for the cation host to compromise the large change in electric field upon the insertion of the MV cations [35].

The galvanostatic charge/discharge curves of $LiV_2(PO_4)_3$ between 0.2 V and 1.9 V is shown in Figure 1c. Even when cycled at the rate as high as 2 C, the charge/discharge curves at different cycles almost overlapped with each other. Such excellent reversibility of Zn^{2+}-entry/exit in $LiV_2(PO_4)_3$ and the accompanying high rate capability are very rare and impressive. A reversible capacity of 141 mAh/g at average discharge potential of around 1.3 V vs Zn was obtained, corresponding to an energy density of 183 Wh/kg. Based on the electrochemical performance, the overall reaction could be described as following:

$$LiV_2(PO_4)_3 + 0.5Zn^{2+} + e^- \rightarrow Zn_{0.5}LiV_2(PO_4)_3,\ \Delta G^{DFT} = -145.49975\ kJ/mol$$

The overall Gibbs free energy calculated through DFT simulation is -145.49975 kJ/mol. It should also be noted that, since Vanadium could be reduced from V^{4+} to V^{3+} or even a lower valence, as reported previously that $Li_3V_2(PO_4)$ could be utilized as either cathode through V^{4+}/V^{3+} redox reaction or anode through V^{3+}/V^{2+} redox reaction[31], the inserted amount of Zn^{2+} in the $LiV_2(PO_4)_3$ lattice could be slightly higher than 0.5. The capacity slightly increases after initial activation process and eventually stabilizes to 168 mAh/g after 30 cycles (Figure S8), corresponding to a high energy density of 218 Wh/kg. When the discharge cut-off voltage is lifted from 0.2 V to 0.8 V, capacity decreases to 98 mAh/g (Figure S9). The discharge curves in Figure 1c display two obvious plateaus at ~1.75 V and ~1.3 V, respectively, with a small slope plateau at 0.5 V, which is shown in a more pronounced manner by the differential capacity curve in Figure S10. The two plateaus represent typical step-wise two-phase transformation behavior. The element mapping for the fully zincated (0.2 V) sample confirms the existence of Zn in the $LiV_2(PO_4)_3$ host (Figure S11 & S12). The Zn^{2+}-insertion in $LiV_2(PO_4)_3$ electrodes was also unequivocally confirmed by the Zn K-edge X-ray absorption spectroscopy (XAS) on the fully zincated $LiV_2(PO_4)$ (Figure 1d). Compared with the $Zn(OTf)_2$ salt, it becomes clear that the Zn spectrum is not caused by the salt, and Zn in the LVP has slightly lower valence than +2. While X-ray absorption near edge structure (XANES, Figure 1d) reveals that ionic Zn^{2+} is present in the host structure, X-ray absorption fine structure (EXAFS, Figure S13) further displays that Zn is bonded with ligand anion with first neighbor distance around 2.0 Å. The charge redistribution after zincation was confirmed by the local charge density difference isosurfaces (Figure 1e) using DFT calculation, showing that the charge around Zn sites decreases significantly while the V and part of the O sites undergo the charge increase. The calculation also confirms that the inserted Zn cation has an effective charge of 1.336, which is smaller than its nominal charge of 2 by more than 30%, in good agreement with the XANES result and suggesting that Zn cation has limited interaction with the anions in the structure, rendering its potential high mobility. It should be mentioned that the radius of Zn^{2+} (0.74 Å) is even slightly smaller than that of Li^+ (0.76 Å), which makes the charge redistribution a much more critical factor for the facile Zn^{2+}-kinetics.

Figure 1f displays the cycling stability and coulombic efficiency of $LiV_2(PO_4)_3$ electrode at both 2 C and 10 C rates. Excellent cycling stability with capacity decay rates of 0.028% and 0.0053% was recorded at 2 C for 500 cycles or at 20 C for 4000 cycles, respectively. A high coulombic efficiency of 100% is achieved after the initial several cycles at both 2 C and 10 C rates. Even at a very low rate of 0.1C, which is usually very challenging for aqueous batteries, the CE gradually increased along with the cycles from 83% of the 1st cycle to 98% of the 10th cycle (Figure S14). Optimizing the stability window of electrolytes could further improve the CE [36]. At an elevated temperature of 55 °C, the $LiV_2(PO_4)_3$ electrode can still maintain 89.9% of the initial capacity at 2 C after 200 cycles (Figure S15). Although the evolution of XRD patterns shows certain decrease in the particle size and slight structural change (Figure S16), such excellent electrochemical reversibility makes it a promising aqueous Zn battery chemistry.

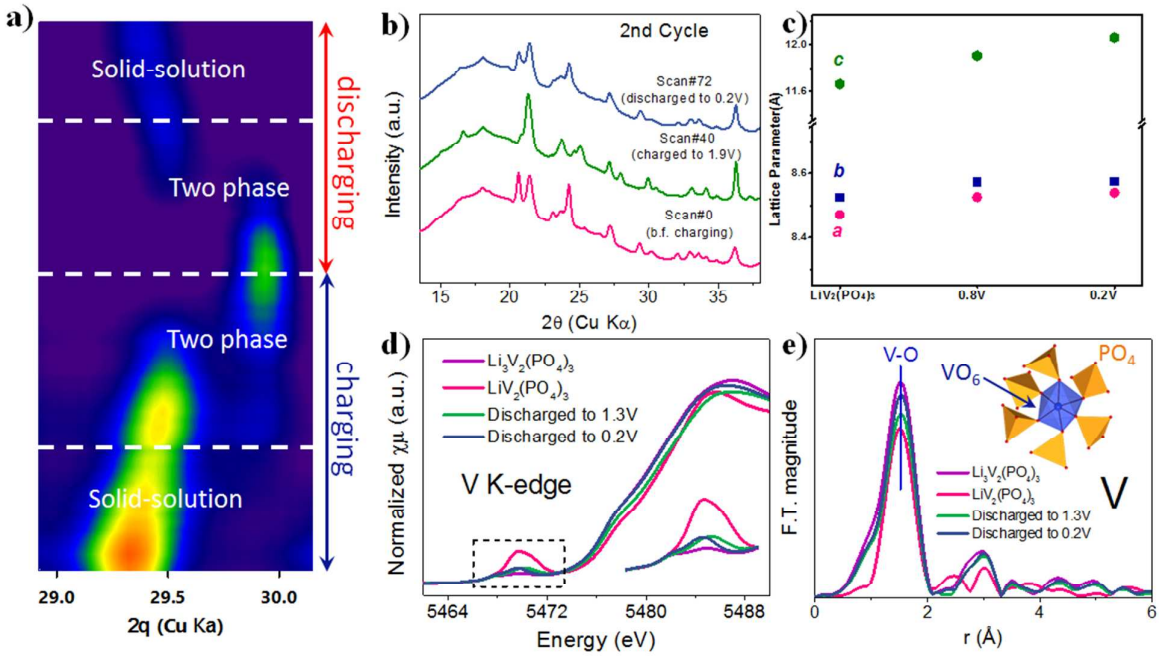

Figure 2. The origin of the excellent reversibility. (a) The *operando* XRD measurement during the second electrochemical cycle showing the XRD pattern evolution as a function of intercalated Zn^{2+} concentration. (b) XRD comparisons of different cycles during the operando measurement. (c) Changes in lattice parameters a, b and c in $LiV_2(PO_4)_3$ electrode at different discharge states. (d) XANES spectra and (e) Fourier-transformed EXAFS spectra collected at the V K-edge of $LiV_2(PO_4)_3$ electrode at different discharge states.

To understand the origin of such unexpected high reversibility, the structure evolution of the $LiV_2(PO_4)_3$ during Zn^{2+} intercalation/de-intercalation was investigated using *in-operando* X-ray diffraction (XRD). When Zn^{2+} leaves the lattice (charging), a continuous peak shift was observed in the low voltage region, implying a solid-solution process (Figure 2a), after which a typical two-phase transition followed. The solid-solution and the two-phase transition are well consistent with the electrochemical characterization (Figure 1c). The *in-operando* XRD patterns of pristine $LiV_2(PO_4)_3$, at both fully charged and discharged states, clearly illustrate the structural reversibility of electrochemical reaction that accommodates Zn^{2+} (Figure 2b). Changes in lattice of $LiV_2(PO_4)_3$ during the discharge was obtained by refining XRD data (Figure S17). Slight increase in lattice parameters *a, b* and *c* were observed during Zn^{2+} insertion, corresponding to a total volume expansion of 5% (Figure 2c and Table S1). Such a small change in unit cell volume is accompanied by oxidization and reduction of V as shown in Figure 2d, and ensures the excellent reversibility of the Zn^{2+}-intercalation chemistry in $LiV_2(PO_4)_3$ cathode host. Even after full zincation, the volume of $Zn_{0.5}LiV_2(PO_4)_3$ is still less than that of the parent $Li_3V_2(PO_4)_3$ phase. The volume contraction after replacing two Li^+ with one Zn^{2+} is ascribed to the stronger electrostatic effect of Zn^{2+}. After removing the intercalated Zn^{2+} (charged to 1.9V), the volume contracted by 3%, confirming the good structure reversibility.

The XANES spectra in Figure 2d also reveal that, during the *in-situ* electrochemical delithiation of $LiV_2(PO_4)_3$ from $Li_3V_2(PO_4)_3$, the edge position shifts from left to right, an indication of the V oxidation. However, upon Zn^{2+}-insertion, the edge position shifts from right to left, indicating that V is reduced back. The total edge energy change from $LiV_2(PO_4)_3$ to $Zn_{0.5}LiV_2(PO_4)_3$ is around 1.2 eV, suggesting that the valence of V changes by ~1 during redox reaction [37], which is in good agreement with the delivered capacity of $Zn_{0.5}LiV_2(PO_4)_3$. From the first charging (de-lithiation) of parent $Li_3V_2(PO_4)_3$ to the charged state $LiV_2(PO_4)_3$, V experiences considerable local environment changes (mostly likely the distortion of VO_6 octahedral), which can be seen from both the substantial increase in pre-edge peak intensity (inset graph of Figure 2d) and the significant reduction of first peak intensity of the Fourier transformed EXAFS data (Figure 2e). After discharge, the pre-edge peak becomes weak again, but is still stronger than that of the pristine state. Similarly, the first peak of Fourier transformed EXAFS data regains intensity, but remains weaker than that of the pristine state. These observations suggest that the local environment of V is not fully restored after the first Zn^{2+} insertion, probably due to the existence of many vacancies created as less number of Zn^{2+} was inserted than that for Li^+ extracted. Based on these unequivocal evidences, we conclude that reversible Zn^{2+}-intercalation chemistry indeed occurs in a polyanion framework, which has been believed impossible hitherto.

The high robustness of the polyanion $LiV_2(PO_4)_3$ structure during Zn insertion/extraction as found by *operando* XRD, XANES and EXAFS might be a unique property for all polyanion family materials. Therefore, a series polyanion cathodes with different crystal structure were also explored. As a well-known olivine compound, delithiated $LiFePO_4$ was selected as Zn^{2+} cathode host, whose reversible reaction with Zn^{2+} was indeed observed (Figure S18a) but with a large overpotential during Zn^{2+}-insertion/extraction and very sluggish reaction kinetics. Similar behavior was also observed in $LiMn_{0.8}Fe_{0.2}PO_4$ (Figure S18b). The DOS of $FePO_4$ and $MnPO_4$ do not show either *p-d* hybridization or small band gap (Figure S18c & d), consistent with the slow reaction kinetics of these two compounds. Theoretically, all polyanion compounds with different crystal structures could reversibly accommodate Zn^{2+}; however, the reaction kinetics are closely related to the structure and the 3d-metal M^{n+}/M^{n+1} redox couples.

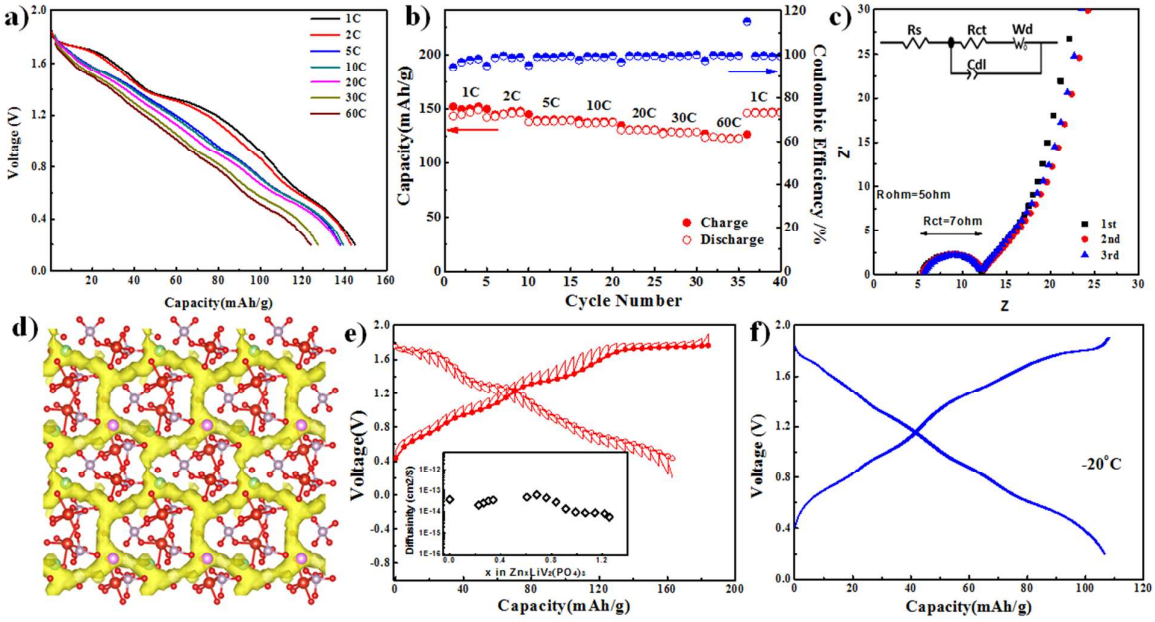

Journal Name

COMMUNICATION

Figure 3. **The fast kinetics of $LiV_2(PO_4)_3$ cathode.** (a) Discharge profiles of $LiV_2(PO_4)_3$ cathode at various C rates (Areal mass loading: 10 mg/cm^2; 140 mA/g as 1 C). (b) The rate capability of $LiV_2(PO_4)_3$ cathode. (c) Nyquist plots for $LiV_2(PO_4)_3$ cathode obtained by electrochemical impedance spectroscopy (EIS) at the fully discharged state during the first three cycles (inset: the equivalent circuit). (d) The structural insights and the Zn diffusional pathway within $LiV_2(PO_4)_3$ framework. (e) The galvanostatic intermittent titration technique (GITT) discharge-charge curve of $LiV_2(PO_4)_3$ in 4 m $Zn(OTf)_2$ aqueous electrolyte. Rest: 1 h; Discharge: 2 min; Current density: 1C (inset the corresponding chemical diffusion coefficient for Zn). (f) The typical voltage profile of $LiV_2(PO_4)_3$ between 0.2 V and 1.9 V at the low temperature of -20 ^{o}C at the rate of 2 C.

Rate capability tests of $LiV_2(PO_4)_3$ electrode corroborated its high power density for Zn^{2+}-intercalation chemistry (Figure 3a). From 1 C to 20 C, only negligible capacity reduction was observed with a remarkably small polarization, leading to little change in energy density. Even at the astonishing rate of 60 C (i.e., fully charge and discharge in 1 min), a high discharge capacity of 122 mAh/g was still maintained, which retains 83.5% of the capacity at 1 C, corresponding to a remarkable power density of 8200 W/kg. Such power performance is further confirmed by continuous cycling at various rates (Figure 3b), where the specific capacity slightly drops when subject to high rates, but immediately recovers when the rate is reduced.

The kinetics of $Zn/LiV_2(PO_4)_3$ full cell is dictated by the rate of Zn^{2+}-intercalation chemistry at the cathode, as shown by the overpotential test in Figure S19. The electrochemical impedance spectra (EIS) conducted at the fully discharged state of cathode indicated the presence of an almost constant interphase component during the cycling (Figure 3c), where the EIS responses from different cycles are completely overlapped. The low ohmic resistance (5 ohm) indicates a low internal resistance due to the high electrolyte conductivity, while the small charge-transfer resistance (7 ohm) confirms that the reaction proceeds at very fast rate. The sloping line at the low frequency region standing for the diffusion-controlled process is consistent with the cyclic voltammetry (CV) results in Figure S20 [38].

The Zn^{2+}-diffusion pathway was also calculated using first-principles method (Figure 3d), which reveals that, despite its bivalence, Zn^{2+}-diffusion share the same one-dimensional pathway with the monovalent Li^+ in the *ab* plane of $LiZn_xV_2(PO_4)_3$ with low activation barriers[39]. The activation energy barriers for Zn^{2+} and Li^+ in $LiZn_{0.25}V_2(PO_4)_3$ as computed from the Arrhenius plots are 484 meV and 212 meV, respectively (Figure S21). Those numbers are comparable with those of Li^+-diffusion in spinel phase $Li_4Ti_5O_{12}$[37], which is known as one of the fastest Li^+-intercalation hosts. To demonstrate the kinetic behavior of $LiV_2(PO_4)_3$ electrode, galvanostatic intermittent titration technique (GITT), which utilizes a relaxation period to maintain the system at quasi-equilibrium state, was conducted. The negligible overpotential (~20 mV) between the transient state and the quasi-equilibrium again confirms the rapid kinetics for Zn^{2+}-intercalation chemistry (Figure 3e). Differing from the general consensus that multivalent chemistries always struggle with sluggish diffusion and charge-transfer, the Zn chemistry demonstrated in this work stands out as an exception. The chemical diffusion coefficient for Zn (D_{Zn}) in $LiV_2(PO_4)_3$ was also calculated from the transient voltage response during the GITT test, which is about 4×10^{-13} cm^{2}s^{-1} in the two-phase area (x<0.8), or 1×10^{-14} cm^{2}s^{-1} in the single-phase region (0.8<x<1.3), well consistent with the diffusivities obtained through the Warburg region fitting of the EIS results (Figure S22). Such values are already higher than that of Li^+ in $FePO_4$ [40] and are doubtless responsible for the excellent rate performance observed. Such facile migration of Zn^{2+} in the close-stacked crystal structure is rarely observed in the multivalent chemistry, which is inspiring not only for Zn but also for other multi-valent chemistries. The exceptionally fast kinetic combined with the decent low temperature properties of the electrolytes gives rise to the excellent capacity retention of $LiV_2(PO_4)_3$ electrode even at low temperature, when 75.8% of the room temperature capacity was retained at -20 ^{o}C (Figure 3f).

Journal Name

COMMUNICATION

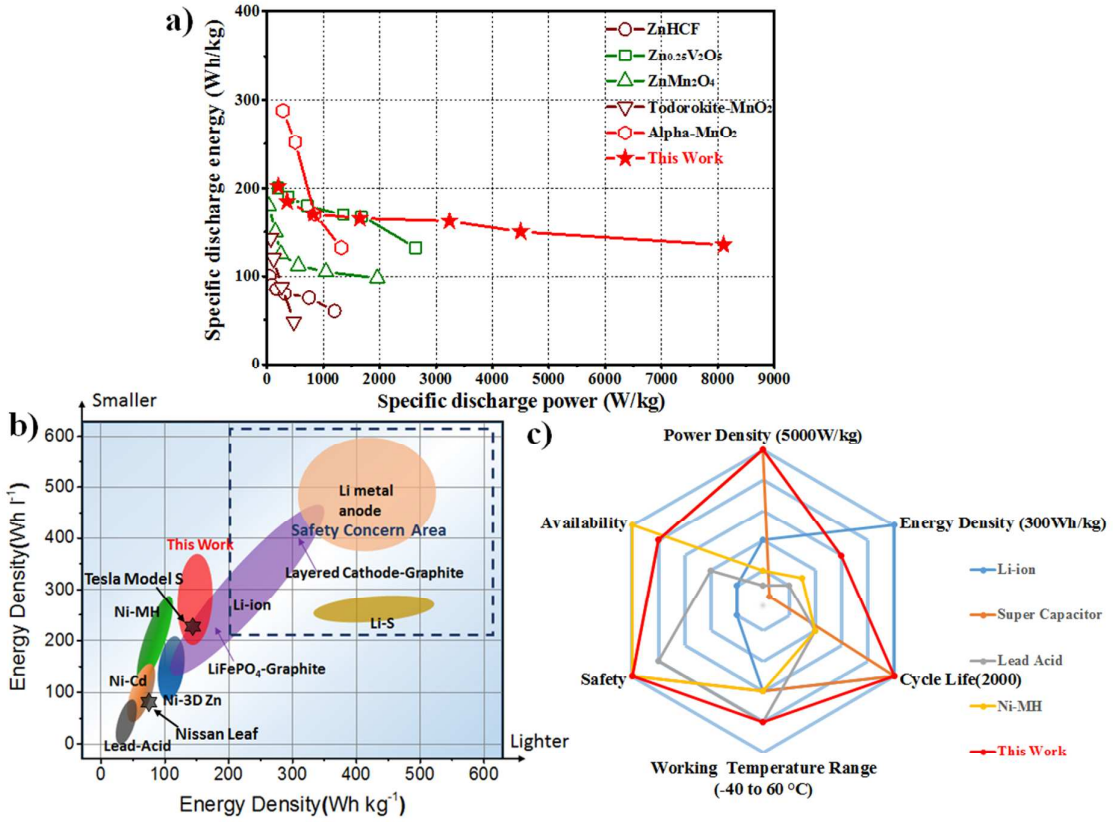

Figure 4. The comprehensive electrochemical performance for $LiV_2(PO_4)_3$. (a) Comparison of $LiV_2(PO_4)_3$ cathode with other known cathode materials for AZIBs. Energy density were calculated based on cathode mass only. (b) Projected cell-level usable gravimetric (Wh/kg) and volumetric (Wh/L) energy densities for different battery systems. (c) The spider chart for the itemized comparison of $Zn/LiV_2(PO_4)_3$ cell with other commercial systems.

To evaluate the electrochemical performances of the $LiV_2(PO_4)_3$ cathode for aqueous Zn-ion battery, the energy and power densities for the typical Zn-ion host cathodes reported in the literature [11, 14- 16, 18, 41] are plotted and compared in Figure 4a. $LiV_2(PO_4)_3$ cathode exhibits the highest power density of 8000 W/kg, comparable to that obtained from supercapacitors. Meanwhile, a steady energy density remains at high level (>150 Wh/Kg) despite the increase in power density. Such superior power and energy performance make it a strong competitor for various energy storage applications, especially where high power density is required to capture or release energy in a short time. Such examples include automotive batteries used in the power train of electric vehicles, or energy storage units used to capture intermittent energy inputs from solar or wind sources in smart grids. On the other hand, as described before, the multivalent battery chemistry is especially attractive because of its high volumetric energy density, which is particularly important for transportation applications. Therefore, we evaluated the energy density of this rechargeable $Zn/LiV_2(PO_4)_3$ cell using a prototype configuration consisting of anode–separator–cathode stacks to occupy a given pouch thickness, which is an identical replica of what used in the work of Aurbach and co-workers[8]. The volumetric and specific energy densities of the different battery systems were summarized in Figure 4b. The cell-level volumetric and specific energy densities achieved in this work are 320 Wh/L and 150 Wh/kg (Table S2), respectively, far exceeding any aqueous batteries commercially available. The volumetric density is even higher than certain LIB systems such as Graphite/$LiFePO_4$ and $Li_4Ti_5O_{12}$/$LiFePO_4$, and close to the state-of-the-art high energy LIBs based on the various NMC chemistries. Even the emerging Li-S chemistry demonstrates lower volumetric energy density than this aqueous Zn system, although its gravimetric energy density is higher. The pack-level energy densities

in current Battery Electric Vehicles (BEVs) range from 90 Wh/L and 70 Wh/kg for Nissan Leaf to 210 Wh/L and 130 Wh/kg for Tesla Model S. Considering the fact that the intrinsic safety of the aqueous chemistry would significantly reduce the need for packaging, protection and battery management system at pack level, $Zn/LiV_2(PO_4)_3$ cells are quite promising candidates for electric vehicle applications.

Figure 4c compares $Zn/LiV_2(PO_4)_3$ chemistry with other well-developed commercial energy storage systems using the six most important parameters, i.e., energy and power densities, cycle-life, service temperature range, safety and materials availability. $Zn/LiV_2(PO_4)_3$ system delivers a high power density that matches supercapacitor while maintaining both high energy density and good cycle life. Such combination of performances is not available from any existing aqueous systems. Though its energy density is still lower than LIBs at the cell level, their superiority in safety makes it possible to make up for the gap at module or pack levels, with simultaneous gains in both safety and manufacturing cost. The fast electrode kinetics and efficient charge transport in $Zn/LiV_2(PO_4)_3$ system ensure high power and fast chargeability at low temperatures, and the robustness of $LiV_2(PO_4)_3$ lattice and aqueous electrolytes maintains the system's good stability even at elevated temperatures.

Conclusions

In conclusion, we demonstrated a very promising ultrafast Zn^{2+}-intercalation chemistry in a close-packed lattice of $LiV_2(PO_4)_3$, where the high charge density of bivalent Zn^{2+} was effectively accommodated by the *p-d* hybridization between the V-*d* and O-*p* orbitals, while Zn^{2+}-diffusion shares a facile pathway with Li^+, resulting in quick kinetics and high power performance. The Zn^{2+}-insertion/extraction in such polyanion-based framework is highly reversible, experiencing only slight volume change and yielding a superior rechargeability. In a rechargeable Zn^{2+} battery, $LiV_2(PO_4)_3$ cathode delivers unprecedented high energy (200 Wh/kg at 1 C) and power (8000 W/kg at 60 C) densities and excellent cycling stability (4000 cycles). The cell-level gravimetric and volumetric energy densities are projected to be 150 Wh/kg and 320 Wh/L, which are even better than the first-generation LIBs. On pack-level, the intrinsic safety of the aqueous nature is expected to eliminate much of the heavily-armed packaging and complicated subsystems required by safety consideration of LIB chemistries, making this aqueous MV battery a competitive candidate for automotive applications.

Conflicts of interest

The authors declare no competing financial interest.

Acknowledgements

The PIs gratefully acknowledge the funding support from DOE ARPA-E (DEAR0000389). The PIs (KX and CSW) gratefully acknowledge the funding support from DOE ARPA-E (DEAR0000389) and Center of Research on Extreme Batteries (CREB). We also acknowledge the support of the Maryland Nano Center and its NispLab. The NispLab is supported in part by the NSF as a MRSEC Shared Experimental Facility. F.W. was supported by the Oak Ridge Associated Universities (ORAU) through contract W911NF-16-2-0202. Enyuan Hu and Xiao-Qing Yang at Brookhaven National Laboratory are supported by the Assistant Secretary for Energy Efficiency and Renewable Energy, Office of Vehicle Technologies of the U.S. Department of Energy through the Advanced Battery Materials Research (BMR) Program, under contract number DE-SC0012704. We gratefully acknowledge the help by beamline scientists Sungsik Lee and Benjamin Reinhart at 12BM and Wenqian Xu at 17BM beamlines of Advanced Photon Source (APS) at Argonne National Laboratory, supported by the U.S. Department of Energy, Basic Energy Science, under Contract No. DE-AC02-06CH11357. This research used beamlines 7-BM of the National Synchrotron Light Source II, a U.S. Department of Energy (DOE) Office of Science User Facility operated for the DOE Office of Science by Brookhaven National Laboratory under Contract No. DE-SC0012704.

references

1. L. Suo, O. Borodin, T. Gao, M. Olguin, J. Ho, X. Fan, C. Luo, C. Wang and K. Xu, *Science*, 2015, **350**, 938-943.
2. B. Dunn, H. Kamath and J.-M. Tarascon, *Science*, 2011, **334**, 928-935.
3. M. Armand and J. M. Tarascon, *Nature*, 2008, **451**, 652-657.
4. J.-Y. Luo, W.-J. Cui, P. He and Y.-Y. Xia, *Nat. Chem.*, 2010, **2**, 760-765.
5. P. Canepa, G. Sai Gautam, D. C. Hannah, R. Malik, M. Liu, K. G. Gallagher, K. A. Persson and G. Ceder, *Chem. Rev.* , 2017, **117**, 4287-4341.
6. Z. Rong, R. Malik, P. Canepa, G. Sai Gautam, M. Liu, A. Jain, K. Persson and G. Ceder, *Chem. Mater.* , 2015, **27**, 6016-6021.
7. Y. Gu, Y. Katsura, T. Yoshino, H. Takagi and K. Taniguchi, *Sci Rep*, 2015, **5**, 12486.
8. J. W. Choi and D. Aurbach, *Nature Reviews Materials*, 2016, **1**, 16013.
9. J. F. Parker, C. N. Chervin, I. R. Pala, M. Machler, M. F. Burz, J. W. Long and D. R. Rolison, *Science*, 2017, **356**, 415-418.
10. P. Senguttuvan, S.-D. Han, S. Kim, A. L. Lipson, S. Tepavcevic, T. T. Fister, I. D. Bloom, A. K. Burrell and C. S. Johnson, *Adv.Energy.Mater*, 2016, **6**, 1600826.
11. D. Kundu, B. D. Adams, V. Duffort, S. H. Vajargah and L. F. Nazar, *Nature Energy*, 2016, **1**, 16119.
12. S. Selverston, R. F. Savinell and J. S. Wainright, *J. Electrochem. Soc.*, 2017, **164**, A1069-A1075.
13. H. Pan, Y. Shao, P. Yan, Y. Cheng, K. S. Han, Z. Nie, C. Wang, J. Yang, X. Li, P. Bhattacharya, K. T. Mueller and J. Liu, *Nature Energy*, 2016, **1**, 16039.
14. C. Xu, B. Li, H. Du and F. Kang, *Angewandte Chemie*, 2012, **51**, 933-935.
15. J. Lee, J. B. Ju, W. I. Cho, B. W. Cho and S. H. Oh, *Electrochim. Acta* 2013, **112**, 138-143.

16. M. H. Alfaruqi, V. Mathew, J. Gim, S. Kim, J. Song, J. P. Baboo, S. H. Choi and J. Kim, *Chem. Mater.* , 2015, **27**, 3609-3620.
17. M. S. Chae, J. W. Heo, S. C. Lim and S. T. Hong, *Inorg. Chem.* , 2016, **55**, 3294-3301.
18. N. Zhang, F. Cheng, Y. Liu, Q. Zhao, K. Lei, C. Chen, X. Liu and J. Chen, *J. Am. Chem. Soc.* , 2016, **138**, 12894-12901.
19. M. H. Alfaruqi, V. Mathew, J. Song, S. Kim, S. Islam, D. T. Pham, J. Jo, S. Kim, J. P. Baboo, Z. Xiu, K.-S. Lee, Y.-K. Sun and J. Kim, *Chem. Mater.* , 2017, **29**, 1684-1694.
20. P. He, M. Yan, G. Zhang, R. Sun, L. Chen, Q. An and L. Mai, *Adv.Energy.Mater*, 2017, 1601920.
21. G. Li, Z. Yang, Y. Jiang, C. Jin, W. Huang, X. Ding and Y. Huang, *Nano Energy*, 2016, **25**, 211-217.
22. J. B. Goodenough and Y. Kim, *Chem. Mater.* , 2010, **22**, 587-603.
23. B. Kang and G. Ceder, *Nature*, 2009, **458**, 190-193.
24. S. Nishimura, G. Kobayashi, K. Ohoyama, R. Kanno, M. Yashima and A. Yamada, *Nat. Mater.* , 2008, **7**, 707-711.
25. H. B. Zhao, C. J. Hu, H. W. Cheng, J. H. Fang, Y. P. Xie, W. Y. Fang, T. N. Doan, T. K. Hoang, J. Q. Xu and P. Chen, *Sci Rep*, 2016, **6**, 25809.
26. J. Yoon, S. Muhammad, D. Jang, N. Sivakumar, J. Kim, W.-H. Jang, Y.-S. Lee, Y.-U. Park, K. Kang and W.-S. Yoon, *Journal of Alloys and Compounds*, 2013, **569**, 76-81.
27. J. Kang, V. Mathew, J. Gim, S. Kim, J. Song, W. B. Im, J. Han, J. Y. Lee and J. Kim, *Sci Rep*, 2014, **4**, 4047.
28. J. Gaubicher, C. Wurm, G. Goward, C. Masquelier and L. Nazar, *Chem. Mater.* , 2000, **12**, 3240-3242.
29. S.-C. Yin, H. Grondey, P. Strobel, M. Anne and L. F. Nazar, *J. Am. Chem. Soc.* , 2003, **125**, 10402-10411.
30. N. V. Kosova, E. T. Devyatkina, A. B. Slobodyuk and A. K. Gutakovskii, *Journal of Solid State Electrochemistry*, 2013, **18**, 1389-1399.
31. Z. Jian, W. Han, Y. Liang, Y. Lan, Z. Fang, Y.-S. Hu and Y. Yao, *J. Mater. Chem. A*, 2014, **2**, 20231-20236.
32. H. Huang, S. C. Yin, T. Kerr, N. Taylor and L. F. Nazar, *Adv. Mater.* , 2002, **14**, 1525-1528.
33. S. Shi, L. Liu, C. Ouyang, D.-s. Wang, Z. Wang, L. Chen and X. Huang, *Physical Review B*, 2003, **68**, 195108.
34. F. Zhou, K. Kang, T. Maxisch, G. Ceder and D. Morgan, *Solid State Commun.* , 2004, **132**, 181-186.
35. Q. D. Truong, M. Kempaiah Devaraju, D. N. Nguyen, Y. Gambe, K. Nayuki, Y. Sasaki, P. D. Tran and I. Honma, *Nano Lett.* , 2016, **16**, 5829-5835.
36. F. Wang, O. Borodin, T. Gao, X. Fan, W. Sun, F. Han, A. Faraone, J. A. Dura, K. Xu and C. Wang, *Nat. Mater.* , 2018, **17**, 543.
37. L. Wang, J. Xu, C. Wang, X. Cui, J. Li and Y.-N. Zhou, *RSC Advances*, 2015, **5**, 71684-71691.
38. V. Augustyn, J. Come, M. A. Lowe, J. W. Kim, P.-L. Taberna, S. H. Tolbert, H. D. Abruña, P. Simon and B. Dunn, *Nat. Mater.* , 2013, **12**, 518-522.
39. S. Lee and S. S. Park, *The Journal of Physical Chemistry C*, 2012, **116**, 25190-25197.
40. Y. Zhu, Y. Xu, Y. Liu, C. Luo and C. Wang, *Nanoscale*, 2013, **5**, 780-787.
41. L. Zhang, L. Chen, X. Zhou and Z. Liu, *Adv.Energy.Mater*, 2015, **5**, 1400930.

The bivalence of Zn^{2+} was delocalized by the multiple atoms through the *p*-*d* hybridization, rendering its high mobility.